HHS Public Access

Author manuscript

*J Am Chem Soc*. Author manuscript; available in PMC 2019 August 01.

Published in final edited form as:

*J Am Chem Soc*. 2018 August 01; 140(30): 9566–9573. doi:10.1021/jacs.8b04641.

# Enzymatic Assemblies Disrupt Membrane and Target Endoplasmic Reticulum (ER) for Selective Cancer Cell Death

**Zhaoqianqi Feng**[†], **Huaimin Wang**[†], **Shiyu Wang**[‡], **Qiang Zhang**[§], **Xixiang Zhang**[§], **Avital Rodal**[‡], and **Bing Xu**[*,†]

[†]Department of Chemistry, Brandeis University, 415 South Street, Waltham, Massachusetts 02454, United States.

[‡]Department of Biology, Brandeis University, 415 South Street, Waltham, Massachusetts 02454, United States.

[§]Physical Science and Engineering Division (PSE), King Abdullah University of Science and Technology (KAUST), Thuwal 23955–6900, Saudi Arabia

## Abstract

The endoplasmic reticulum (ER) is responsible for the synthesis and folding of a large number of proteins, as well as intracellular calcium regulation, lipid synthesis, and lipid transfer to other organelles, and is emerging as a target for cancer therapy. However, strategies for selectively targeting the ER of cancer cells are limited. Here we show that enzymatically generated crescent-shaped supramolecular assemblies of short peptides disrupt cell membranes and target ER for selective cancer cell death. As revealed by sedimentation assay, the assemblies interact with synthetic lipid membranes. Live cell imaging confirms that the assemblies impair membrane integrity, which is further supported by lactate dehydrogenase (LDH) assays. According to transmission electron microscopy (TEM), static light scattering (SLS), and critical micelle concentration (CMC), attaching an L-amino acid at the C-terminal of a D-tripeptide results in the crescent-shaped supramolecular assemblies. Structure activity relationship suggests that the crescent-shaped morphology is critical for interacting with membranes and for controlling cell fate. Moreover, fluorescent imaging indicates that the assemblies accumulate on ER. Time-dependent Western blot and ELISA indicate that the accumulation causes ER stress and subsequently activates the caspase signaling cascade for cell death. As an approach for in-situ generating membrane binding scaffolds (i.e., the crescent-shaped supramolecular assemblies), this work promises a new way to disrupt membrane and to target ER for developing anticancer therapeutic.

[*]**Corresponding Author:** bxu@brandeis.edu.

ASSOCIATED CONTENT

Materials, detailed experimental procedures, additional figures and videos. This material is available free of charge via the Internet at http://pubs.acs.org.

The authors declare no competing financial interest.

## Introduction

Organelle targeting has emerged as a promising strategy in developing effective and specific cancer therapeutics.[1] By delivering a drug in its active form to the cellular compartment, organelle targeting increases drug concentration at the target where the drug acts, thus improving the effectiveness and reducing side effects.[2] The past few years have seen the advance of strategies for targeting different organelles, including the nucleus, mitochondria,[3] lysosomes,[4] and the endoplasmic reticulum (ER).[5] Among these subcellular targets, ER targeting therapy has been little explored due to its complexity in cell signaling.[6] As the largest cellular organelle, ER is responsible for crucial biosynthetic, sensing, and signaling functions in eukaryotic cells.[7,8] Particularly, ER is responsible for the synthesis, folding, and posttranslational modifications of proteins destined for the secretory pathway, which amount to approximately 30% of the total proteome.[9] Disturbing the protein-folding capacity of ER would result in ER stress, ultimately activating apoptotic signaling pathways and cell death. Therefore, selective disrupting ER function in cancer cells is a promising new strategy for anticancer therapies.[10] However, current ER targeting small molecules, like tunicamycin and thapsigargin, lack cell selectivity and exhibit severe neurotoxicity, thus hindering their clinical applications.[11] One way to target ER is to conjugate drugs to protein toxins (e.g., Shiga toxin) which allows the delivery of drugs to ER.[1] However, such endocytosis-dependent delivery still faces the difficulty in achieving endosome/lysosome escape. Therefore, it is necessary to develop novel ER targeting strategies that have high specificity against cancer cells. To meet this need, we decided to explore enzyme-instructed self-assembly (EISA)[12,13] for ER targeting because EISA provides precise spatiotemporal control.

EISA is a dynamic process prevalently utilized for regulating proteins in nature,[14] and is also applicable for small molecules. In fact, EISA of peptides[15], lipids[16], carbohydrates,[17] or sterol[18] has already shown great promise as a potential cancer therapy for selectively inhibiting cancer cells. Because specific enzymes are enriched in cancer cells and localize at certain subcellular locations, EISA localizes the supramolecular assemblies at the location of the enzymes; the formed assemblies significantly reduce the diffusion and greatly increase the diffusion-limited interaction.[19] This unique advantage of EISA has made it an attractive strategy to target different subcellular organelles, including the cell membrane,[20] nucleus,[21] and mitochondria,[22] for boosting accumulation and efficacy of small molecules. For example, targeting mitochondria by EISA minimizes acquired drug resistance.[23] These results also support the development of EISA to selectively target ER in cancer cells, which has yet to be examined.

This study shows that enzymatic supramolecular assemblies from a phosphotetrapeptide (**1P**) disrupt cell membrane and target ER to result in cancer cell death (Scheme 1). Following dephosphorylation by an ectoenzyme, alkaline phosphatase (ALP), **1P** turns into a tetrapeptide derivative (**1**). Assemblies of **1** form via non-covalent interactions, and self-assemble into crescent-shaped aggregates on the cancer cell surface, and interact with lipid membrane to directly disrupt the integrity of the cells. After being taken up by the cancer cells, the assemblies of **1** accumulate at the ER and induce ER stress, which leads to cancer cell death by activating caspase signaling cascade.[24] Examining the analogues of **1P** reveals

that attaching an L-amino acid at the C-terminal of a D-tripeptide causes the crescent-shaped morphology of the assemblies. The crescent-shaped morphology of the assemblies is critical for selectively inhibiting cancer cells because such a morphology results in membrane disruption and leakage (Scheme 1). This work, for the first time, demonstrates a reaction-based process for disrupting membranes in a spatiotemporally controlled manner, as well as subcellular organelle (i.e., ER) targeting, which illustrates a new concept in controlling cell fates via instructed-assembly.[13]

## Results and Discussion

### Molecule design and synthesis.

Scheme 1 shows the structure of the EISA precursor **1P**, which consists of (i) a D-peptidic backbone D-Phe-D-Phe as the self-assembling motif with excellent biostability, (ii) a D-phosphotyrosine to serve as a substrate of ALP, (iii) an N-terminal capping 2-naphthylacetyl group to enhance aromatic–aromatic interactions, and (iv) a positively charged L-homoarginine residue to promote membrane interaction.[25] Because ER is the largest membranous structure inside cells (constituting more than half of the total membrane of a cell[26]), such a design allows ER targeting by the enzymatic assemblies to interact the ER membrane. To examine the roles of side chain length and stereochemistry associated with homoarginine, we design and synthesize precursor **2P** and **3P** as the controls of **1P** (Scheme S1). Specifically, **2P** has an L-arginine with a side chain one methylene less than that of homoarginine. As a diastereomer of **2P**, **3P** contains D-arginine to replace the L-arginine (in **2P**). The designed precursors are synthesized via solid-phase peptide synthesis[27] by using Fmoc-protected amino acids and Fmoc-D-Tyr($PO_3H_2$)-OH prepared by the N-Fmoc protection[28] of phospho-D-tyrosine (Scheme S2). After high-performance liquid chromatography (HPLC) purification, NMR spectra and LC–MS analysis (Figure S1–10) confirm the structures and purities of the designed precursors.

### Enzymatic self-assembly *in vitro*.

To examine the ALP instructed self-assembly of **1**, we utilize high-resolution transmission electron microscopy (HRTEM) to reveal the nanostructures in the solution of **1P** and in the hydrogel formed by treating **1P** with ALP (Figure S11). As shown in Figure 1A, at a concentration of 0.5 wt%, **1P** forms uneven nanoparticles while the enzymatic dephosphorylation (Figure S12) results in crescent-shaped assemblies with an average inner diameter of 8.1 ± 0.9 nm and a width of 5.2 ± 0.6 nm. Static light scattering (SLS) results show that the solutions of **1P** exhibit little SLS signal at the concentrations below 200 μM (Figure 1B), suggesting that **1P** scarcely forms any assemblies at these concentrations. This result agrees with that the critical micelle concentration (CMC) of **1P** is about 272 μM (Figure S13). After the addition of ALP, the SLS signal of **1P** (20–500 μM) increases significantly in a concentration dependent manner, agreeing with that the CMC of **1** **(**generated by treating **1P** with ALP) is about 18.1 μM (Figure S13). Notably, the crescent morphology persists when the concentration of **1** (generated by dephosphorylation **1P**) decreases (Figure S14), indicating that the morphology of the assemblies of **1** likely is independent to the concentration of **1**. These results, together with the TEM images, confirm the formation of crescent-shaped assemblies by enzymatically converting **1P** to **1**.

### Selective anticancer activities.

Incubation of **1P** with three ALP expressing cancer cell lines—cervical cancer cells (HeLa), cisplatin-resistant ovarian cancer cells (A2780cis), and high-grade serous ovarian cancer cells (OVSAHO)[29,30]—reveals that **1P** potently inhibits survival of HeLa, A2780cis, and OVSAHO cells with an $IC_{50}$ of 24, 49, and 54 μM, respectively. The $IC_{50}$ values (Figure 2) largely correlate with the ALP expression levels on these cells.[30] To evaluate the selectivity of **1P**, we also test its toxicity on a normal stromal cell line (HS-5),[31] which expresses relatively low level of ALP, and find that the $IC_{50}$ of **1P** on HS-5 cells is above 500 μM (Figure 2). These results validate that the selectivity of **1P** towards cancer cells mainly originates from the ALP expression on cancer cells. Contrary to the high anticancer efficacy of **1P**, molecules of **1** exhibit minimal cytotoxicity to these three types of cancer cells, even at a concentration of 500 μM (Figure 2), suggesting the importance of enzymatic dephosphorylation in inducing death of the cancer cells. Moreover, the addition of exogenous ALP, a PLAP inhibitor (L-phenylalanine),[32] and a TNAP inhibitor (DQB)[33] rescues the HeLa cells treated with **1P** (200 μM), increasing the cell viability from 20% to 85%, 36%, and 51%, respectively (Figure S16). Additionally, the combination of the PLAP inhibitor and the TNAP inhibitor increases the cell viability of HeLa cells from 20% to 71%, (Figure S16), agreeing with the expression of both PLAP and TNAP in HeLa cells.[30] These results confirm that EISA process is the major contributor of the cancer cell death.

### Membrane interaction and disruption.

To examine the membrane-binding capability of the assemblies generated from catalytic dephosphorylation of **1P**, we perform liposome co-sedimentation assays[34] with liposomes containing phosphatidylinositol 4,5-bisphosphate ($PIP_2$) at the concentration of 1%.[35] While **1P** itself binds poorly to the liposomes, the enzymatically formed assemblies of **1** exhibit membrane-binding affinity with about 90% of **1** bound to the liposomes (Figure 3A). This result suggests that the interactions between the assemblies of **1** and the cell membrane may contribute to cytotoxicity.[36] To test this hypothesis, we measure the leakage of the cytoplasmic enzyme LDH into the culture medium, an indicative assay of plasma membrane disintegration.[37] We choose HeLa cells for the mechanistic studies because **1P** potently inhibits HeLa cells, a cell line that has served as a model of human cell biology for decades.[38] As shown in Figure 3B, **1P** induces LDH release from the HeLa cells in a dose and time-dependent manner. Specifically, when the concentration of **1P** rises from 20 μM to 200 μM, the percentage of released LDH increases from 2.1% to 12.2% and from 3.6% to 16.4% after 0.5 and 1 h incubation, respectively. These results, together with the liposome co-sedimentation, confirm that the enzymatic assemblies of **1** disrupt the cell membranes. Additionally, incubation of HeLa cells with **1P** (200 μM) leads to the LDH release from the HeLa cells within half an hour, suggesting that the disruption of cellular membranes occurs rapidly.

To trace the dynamic interaction of **1P** with the plasma membrane, we use time-lapse microscopy to image changes in the HeLa cell membrane induced by **1P** (200 μM) after staining the cells with a membrane probe.[39] Adding **1P** to the HeLa cells rapidly changes the plasma membrane dynamics and induces membrane curvature[40] and tubulation, as evidenced by the live cell imaging (Video S1). With the probe but without the addition of

**1P**, the cells hardly exhibit tubulation.[39] Specifically, after only 15 minutes of incubation, curvature initiated from the edge of the plasma membrane (white arrows in Figure 4), agreeing with the rapid membrane disruption and LDH leakage (Figure 3B). In addition, the membrane tubules, formed via treating with **1P**, grow with the increase of the incubation time (pink arrows in Figure 4). Providing direct visualization of the dynamic changes of plasma membrane, these results further confirm that **1P** starts to transform into the assemblies of **1** on cell surface, thus disrupting the cell membranes.

## Crescent-shaped morphology is critical for membrane disruption and cancer cell inhibition.

To understand how the molecular structure affect the anticancer efficacy and selectivity of **1P**, we measure the inhibitory activities of the analogs of **1P** on HeLa and HS-5 cells (Figure 5). While **1P** potently inhibits HeLa cells, precursor **2P**, generated by using L-arginine to replacing the L-homoarginine residue in **1P**, exhibits less cytotoxicity ($IC_{50}$ of 180 μM (Figure 5A)). The difference between the activities of **1P** and **2P** likely originates from the difference between L-homoarginine and L-arginine, that is, the length of the side chain. As a diastereomer of **2P**, **3P** is almost innocuous to HeLa cells even at 500 μM, suggesting that the stereochemistry plays essential role in the activity of the assemblies. The potency of the precursors at 24 h against HeLa cells follows the order of **1P** > **2P** > **3P**. In contrast to the case of HeLa cells, the $IC_{50}$ values of the precursors against HS-5 cells are all above 500 μM, likely resulted from the low ALP activity on HS-5 cells.[30]

Because the precursors (**1P**, **2P**, and **3P**) share similar molecular structures except the C-terminal residue, we further characterize the morphologies of their enzymatic assemblies (i.e., the assemblies of **2** and **3** made from dephosphorylation of **2P** and **3P**, respectively). HRTEM reveals that slight variations in the C-terminal residues of the precursors (**1P**, **2P**, and **3P**) lead to significant differences in the morphologies of their assemblies after enzymatic dephosphorylation (Figure 6A, Figure S18). The precursor **2P** forms uneven nanoparticles, which transform into short crescent-shaped nanofibers with width of 11 ± 1.0 nm via EISA (Figure 6A, Figure S18). While precursor **3P** self-assembles to form short nanofibers (6.2 nm) and amorphous aggregates (Figure S18), the addition of ALP to the solution of **3P** results in long, uniform nanofibers with a diameter of 8.6 ± 1.5 nm (Figure 6A). These results indicate that the L-amino acid residue at the C-terminal of the D-tripeptide is essential for forming crescent-shaped assemblies.

Despite the difference in the morphologies of the assemblies of precursors (or hydrogelators), the self-assembling abilities of **2P** and **3P** are close (Figure 6B), and are comparable to that of **1P**. Specifically, the CMC values of **2P** and **3P** are 283 μM and 302 μM, respectively. After being generated by the ALP treatment, **2** and **3** exhibit CMCs of 19.3 and 19.8 μM, respectively. The close CMC values of the dephosphorylated molecules (**1**, **2**, and **3**) suggest that their self-assembling ability are close, thus excluding the possibility that the difference in anticancer efficacy originate from the self-assembling ability of the EISA molecules.[14] Therefore, the different supramolecular morphologies likely contribute to the observed difference in anticancer activities of the precursors.

To assess how the supramolecular morphology affects bioactivity of EISA, we evaluate the membrane-binding properties of the assemblies using the liposome co-sedimentation assays since EISA on cell membrane plays crucial role for determining its bioactivity.[14] As shown in Figure 7A, 91 %, 72%, and 43% of the enzymatic assemblies of **1**, **2**, and **3** bind to the liposomes, indicating that the membrane binding ability of these assemblies follows the order of **1** > **2** > **3**. Additionally, the results of LDH assay (Figure 7B) show that the LDH release from the HeLa cells increases when the incubation time of **1P** (or **2P**) increases. But **3P** hardly induces the LDH leakage from HeLa cells. The amount of LDH release, after treating with the precursors, follows the order of **1P** > **2P** > **3P**. This result strongly correlates the cytotoxicities with the membrane disruption abilities of the assemblies. Since the precursors share the similar molecular structures and charge distributions, their different membrane interactions are likely due to their supramolecular structures. These results suggest that supramolecular morphology of EISA contributes to the anticancer activity through the membrane disruption.

### Distribution of the assemblies inside cells.

To visualize the distribution of the enzymatic assemblies inside the cells after the cell membrane loses integrity, we design and synthesize **F1P** (Scheme S1), a fluorescent analogue of **1P**, by replacing the naphthyl group at the N-terminal with an environment sensitive fluorescent dye 4-nitro-2,1,3-benzoxadiazole (NBD).[41] Dephosphorylated by ALP, **F1P** turns into **F1**, which also forms crescent-shaped assemblies (with an average width of 5.1 ± 2 nm, Figure S20). Because NBD has a higher quantum yield in a hydrophobic environment,[42] EISA of **F1P** induces significantly bright fluorescence for visualizing the distribution of enzymatic assemblies in live cells and real-time.

Figure 8 shows the time-lapse images of the generation and distribution of the enzymatic assemblies in cellular environment (also see Video S2). At 0 min incubation, **F1P** slightly fluoresces to give a dim background in the cytosol of HeLa cells. At this moment, a few slightly brighter spots (indicated by the orange arrow) appear on the cell surface. These results confirm **F1P** being outside the cells at 0 min. At 10 min, the number of fluorescent spots on cell surface increases; a membrane blebbing[43] (pointed by the white arrow) starts to grow near the fluorescent spots. This result suggests membrane disruption of HeLa cells, which corresponds with LDH results (Figure 3B). From 20 to 30 min, the number of fluorescent spots on the cell surface increases, and the membrane blebs grow. The generation and growth of fluorescent assemblies on plasma membrane further confirms that the EISA process occurs on cell surface. Additionally, these enzymatic assemblies adhere to the cell membrane and barely diffuse (pink arrow in Figure 8), agreeing with their high membrane binding affinity (Figure 3A). At 40 min, besides the fluorescence dots emerge on cell membrane, the cytoplasm begins to exhibit weak fluorescence. The fluorescence intensity inside the cells is similar to that of the medium, indicating that the molecules in cells are mainly **F1P** at 40 min. From 50 min to 60 min, the fluorescence intensity in the cytoplasm increases significantly, and the fluorescence spots on cell surface continue to grow. At 70 min, the cytoplasm of the cells exhibit bright fluorescence, suggesting that **F1P** transforms to **F1**, and **F1** assemblies and accumulates inside the cells. These results confirm that (i) **F1P** enters the cells; (ii) EISA of **F1P**/**1P** occurs both on and inside the HeLa cells. To delineate

the role of enzyme specificity, we replace the phosphotyrosine in **F1P** with a phosphoserine to generate precursor **F4P** (Scheme S1), which only exhibits weak fluorescence on cell surface and few puncta inside HeLa cells (Figure S21). This result suggests that intracellular tyrosine phosphatases (e.g., PTP1B on ER[44]) also likely catalyze the dephosphorylation of **F1P**. In contrast to the case of HeLa cells, **F1P** scarcely shows fluorescence on HS-5 cells, (Figure S22) further confirming the selective generation of enzymatic assemblies on cancer cells.

### Targeting endoplasmic reticulum.

To investigate the ER targeting of enzymatic assemblies, we use ER-tracker to co-stain with **F1P** in live HeLa cells. After incubating with **F1P** for 1 h, the green fluorescence from the assemblies of **F1** co-localizes well with the red fluorescence from ER-tracker (Figure 9). The Pearson's R value of co-localization[45] is 0.71 from 20 cells, indicating that most of the assemblies accumulate on ER. Additionally, we also find some green fluorescent dots adhere to the HeLa cell membrane. These results, together with live cell image (Video S2), indicate that the EISA process first occur on cell surface to generate enzymatic assemblies. After **F1P** or assemblies of **F1** enter cells, they accumulate on ER.

Because ER is the major site of protein synthesis and processing,[8] the accumulation of enzymatic assemblies may induce ER dysfunction.[46] To test this assumption, we use time-dependent Western blot to examine the expression of the markers of ER stress. Our results (Figures 10 and S23) confirm that treating HeLa cells with **1P** leads to increased levels of ER chaperon protein Bip, sensor protein IRE1α, and UPR mediator CHOP.[47] We speculate that Bip goes down and up likely because Bip is short-lived and metabolized through N-terminal arginylation under cellular stresses.[48] Calnexin, another chaperon protein for assisting protein folding,[49] slightly decreases after 12 h treatment of **1P**, which is likely due to the degradation of calnexin during apoptosis.[49] Incubating with **1P** activates the IRE1α pathway in HeLa cells, as evidenced by the increased expression of XBP-1 and phospho-JNK(Figure S23).[50] Moreover, **1P** also induces the phosphorylation of PERK and eIF2α in HeLa cells, (Figure S23) indicating the activation of PERK signaling.[51] The addition of the antioxidants (N-acetylcysteine), which reduces ER stress,[52] significantly increases the viability of HeLa cells treated with **1P** (Figure S24). Together with that prolonged ER stress leads to cell apoptosis,[53] these results suggest that EISA of **1** acting through the branch of IRE1α and PERK to induce ER stress is one of the mechanisms contributing to the cell death. Moreover, EISA of **1** also induces the activation of caspase-8 (Figure S23), agreeing with the model that ER stress leads to activation of caspase-8.[54] In addition to HeLa cells, **1P** also induces the ER stress and activates caspase 8 on A2780cis cells, as revealed by the Western blot results (Figure S25).

To further explore the signaling molecules involved in apoptosis pathways, we use PathScan apoptosis multi-target sandwich ELISA[55] to detect the changes of their expression. Time-dependent ELISA results (Figure S26) show that caspase-3 and active poly (ADP-ribose) polymerase (PARP) significantly increase after treating HeLa cells with **1P** for 24 h, suggesting that **1P** induces the death of HeLa cells through intrinsic signaling pathways, including caspase cascade and downstream PARP signaling.

## Conclusion

In conclusion, we demonstrate the selective ER targeting of cancer cells by generating supramolecular assemblies via enzymatic reactions on and in the cancer cells. Interacting with cellular membranes, the crescent-shaped supramolecular assemblies disrupt plasma membrane integrity to enable the assemblies accumulate on the ER, thus inducing cancer cell death through ER stress. This result is consistent with that toxic forms of amyloid-related aggregates of proteins bind to membranes[56] and induce ER stress as a major mechanism of cytotoxicity in neurodegenerative diseases.[57] Utilizing enzymatic reactions and reduced diffusion, EISA enables spatiotemporal control of the generation and cellular distribution of the cytotoxic assemblies, thus providing a new strategy to regulate amyloid-like aggregates for treating cancer. Although this work employs short peptides, EISA promises a new strategy to manipulate peptidomimetic molecules that undergo self-assembling.[58] The use of ALP as the enzyme to confer selectivity to cancer cells may also complement to immunotherapy because overexpression of ALP associates with immunosuppression.[59] Besides controlling the cell behavior using EISA that exhibit high affinity to membrane, this work extends the concept of generating functional assemblies through instructed-assembling, which promises new applications of supramolecular chemistry[60] in live systems.[61]

## Supplementary Material

Refer to Web version on PubMed Central for supplementary material.

## ACKNOWLEDGMENT

This work was partially supported by NIH (R01CA142746) and NSF (DMR-1420382).

## REFERENCES

(1). Rajendran L ; Knolker HJ ; Simons K Nat. Rev. Drug Discovery 2010, 9, 29.20043027

(2). Sakhrani NM ; Padh H Drug Des., Dev. Ther 2013, 7, 585.

(3). Muratovska A ; Lightowlers RN ; Taylor RW ; Wilce JA ; Murphy MP Adv. Drug Delivery Rev 2001, 49, 189;Kang BH ; Plescia J ; Dohi T ; Rosa J ; Doxsey SJ ; Altieri DC Cell 2007, 131, 257.17956728

(4). Grabowski GA ; Hopkin RJ Annu. Rev. Genomics Hum. Genet 2003, 4, 403;14527307Liu B ; Turley SD ; Burns DK ; Miller AM ; Repa JJ ; Dietschy JM Proc. Natl. Acad. Sci. U. S. A 2009, 106, 2377.19171898

(5). Johannes L ; Decaudin D Gene Ther 2005, 12, 1360;15902276Aridor M Adv. Drug Delivery Rev 2007, 59, 759;Suntharalingam K ; Johnstone TC ; Bruno PM ; Lin W ; Hemann MT ; Lippard SJ J. Am. Chem. Soc 2013, 135, 14060.24041161

(6). Cubillos-Ruiz JR ; Bettigole SE ; Glimcher LH Cell 2017, 168, 692.28187289

(7). Verfaillie T ; Garg AD ; Agostinis P Cancer Lett 2013, 332, 249.20732741

(8). Schwarz DS ; Blower MD Cell. Mol. Life Sci 2016, 73, 79.26433683

(9). Hetz C Nat. Rev. Mol. Cell Biol 2012, 13, 89.22251901

(10). Boelens J ; Lust S ; Offner F ; Bracke ME ; Vanhoecke BW In Vivo 2007, 21, 215;17436569Healy SJM ; Gorman AM ; Mousavi-Shafaei P ; Gupta S ; Samali A Eur. J. Pharmacol 2009, 625, 234;19835867Nam JS ; Kang MG ; Kang J ; Park SY ; Lee SJC ; Kim HT ; Seo JK ; Kwon OH ; Lim MH ; Rhee HW ; Kwon TH J. Am. Chem. Soc 2016, 138, 10968.27494510

(11). Foufelle F ; Fromenty B Pharmacol. Res. Perspect 2016, 4.

(12). Feng ZQQ ; Zhang TF ; Wang HM ; Xu B Chem. Soc. Rev 2017, 46, 6470;28849819Wang HM ; Feng ZQQ ; Xu B Chem. Soc. Rev 2017, 46, 2421;28357433Zhou J ; Xu B Bioconjugate Chem 2015, 26, 987;Du W ; Hu X ; Wei W ; Liang G Bioconjugate Chem 2018, 29, 826.

(13). He H ; Xu B Bull. Chem. Soc. Jpn 2018, 91, 900.

(14). Feng ZQQ ; Wang HM ; Chen XY ; Xu B J. Am. Chem. Soc 2017, 139, 15377.28990765

(15). Feng ZQQ ; Wang HM ; Du XW ; Shi JF ; Li J ; Xu B Chem. Commun 2016, 52, 6332.

(16). Tanaka A ; Fukuoka Y ; Morimoto Y ; Honjo T ; Koda D ; Goto M ; Maruyama T J. Am. Chem. Soc 2015, 137, 770.25521540

(17). Pires RA ; Abul-Haija YM ; Costa DS ; Novoa-Carballal R ; Reis RL ; Ulijn RV ; Pashkuleva I J. Am. Chem. Soc 2015, 137, 576.25539667

(18). Wang HM ; Feng ZQQ ; Wu DD ; Fritzsching KJ ; Rigney M ; Zhou J ; Jiang YJ ; Schmidt-Rohr K ; Xu B J. Am. Chem. Soc 2016, 138, 10758.27529637

(19). Kholodenko BN ; Hoek JB ; Westerhoff HV Trends Cell Biol 2000, 10, 173.10754559

(20). Sinthuvanich C ; Veiga AS ; Gupta K ; Gaspar D ; Blumenthal R ; Schneider JP J. Am. Chem. Soc 2012, 134, 6210;22413859Versluis F ; van Elsland DM ; Mytnyk S ; Perrier DL ; Trausel F ; Poolman JM ; Maity C ; le Sage VAA ; van Kasteren SI ; van Esch JH ; Eelkema R J. Am. Chem. Soc 2016, 138, 8670.27359373

(21). Cai Y ; Shen H ; Zhan J ; Lin M ; Dai L ; Ren C ; Shi Y ; Liu J ; Gao J ; Yang Z J. Am. Chem. Soc 2017, 139, 2876.28191948

(22). Jeena MT ; Palanikumar L ; Go EM ; Kim I ; Kang MG ; Lee S ; Park S ; Choi H ; Kim C ; Jin S-M ; Bae SC ; Rhee HW ; Lee E ; Kwak SK ; Ryu J-H Nat. Commun 2017, 8.28364116

(23). Wang H ; Feng Z ; Wang Y ; Zhou R ; Yang Z ; Xu B J. Am. Chem. Soc 2016, 138, 16046.27960313

(24). Thornberry NA ; Lazebnik Y Science 1998, 281, 1312;9721091Mason SD ; Joyce JA Trends Cell Biol 2011, 21, 228.21232958

(25). Bechara C ; Sagan S FEBS Lett 2013, 587, 1693.23669356

(26). Shen YH ; Zhao ZL ; Zhang LY ; Shi LY ; Shahriar S ; Chan RB ; Di Paolo G ; Min W Proc. Natl. Acad. Sci. U. S. A 2017, 114, 13394;29196526Nature cell biology Alberts B , J. A , Lewis J , Raff M , Roberts K and Walter P Garland Science, New York 2002, 689.

(27). Merrifield RB J. Am. Chem. Soc 1963, 85, 2149.

(28). Ottinger EA ; Shekels LL ; Bernlohr DA ; Barany G Biochemistry 1993, 32, 4354.7682846

(29). Feng Z ; Wang H ; Zhou R ; Li J ; Xu B J. Am. Chem. Soc 2017, 139, 3950.28257192

(30). Zhou J ; Du X ; Berciu C ; He H ; Shi J ; Nicastro D ; Xu B Chem 2016, 1.

(31). Roecklein BA ; Torokstorb B Blood 1995, 85, 997.7849321

(32). Hoylaerts MF ; Manes T ; Millan JL Biochem. J 1992, 286, 23.1520273

(33). Dahl R ; Sergienko EA ; Su Y ; Mostofi YS ; Yang L ; Simao AM ; Narisawa S ; Brown B ; Mangravita-Novo A ; Vicchiarelli M ; Smith LH ; O'Neill WC ; Millan JL ; Cosford NDP J. Med. Chem 2009, 52, 6919.19821572

(34). Zhao HX ; Lappalainen P Mol. Biol. Cell 2012, 23, 2823.22848065

(35). Anderluh A ; Hofmaier T ; Klotzsch E ; Kudlacek O ; Stockner T ; Sitte HH ; Schuetz GJ Nat. Commun 2017, 8;28364116Czech MP Cell 2000, 100, 603.10761925

(36). Newcomb CJ ; Sur S ; Ortony JH ; Lee OS ; Matson JB ; Boekhoven J ; Yu JM ; Schatz GC ; Stupp SI Nat. Commun 2014, 5.

(37). Bagchi D ; Bagchi M ; Hassoun EA ; Stohs SJ Toxicology 1995, 104, 129.8560491

(38). Masters JR Nat. Rev. Cancer 2002, 2, 315.12001993

(39). Wang H ; Feng Z ; Del Signore SJ ; Rodal AA ; Xu B J. Am. Chem. Soc 2018, 140, 3505.29481071

(40). Lou H-Y ; Zhao W ; Zeng Y ; Cui B Acc. Chem. Res 2018, 51, 1046.29648779

(41). Gao Y ; Shi JF ; Yuan D ; Xu B Nat. Commun 2012, 3.

(42). Mazeres S ; Schram V ; Tocanne JF ; Lopez A Biophys. J 1996, 71, 327.8804615

(43). Fackler OT ; Grosse R J. Cell Biol 2008, 181, 879.18541702

(44). Frangioni JV ; Beahm PH ; Shifrin V ; Jost CA ; Neel BG Cell 1992, 68, 545.1739967

(45). Dunn KW ; Kamocka MM ; McDonald JH Am. J. Physiol.: Cell Physiol 2011, 300, C723.21209361

(46). Kouroku Y ; Fujita E ; Jimbo A ; Kikuchi T ; Yamagata T ; Momoi MY ; Kominami E ; Kuida K ; Sakamaki K ; Yonehara S ; Momoi T Hum. Mol. Genet 2002, 11, 1505.12045204

(47). Tabas I ; Ron D Nat. Cell Biol 2011, 13, 184;21364565Yamaguchi H ; Wang H-G J. Biol. Chem 2004, 279, 45495.15322075

(48). Shim SM ; Choi HR ; Sung KW ; Lee YJ ; Kim ST ; Kim D ; Mun SR ; Hwang J ; Cha-Molstad H ; Ciechanover A ; Kim BY ; Kwon YT Sci. Signaling 2018, 11.

(49). Delom F ; Emadali A ; Cocolakis E ; Lebrun J ; Nantel A ; Chevet E Cell Death Differ 2007, 14, 586.16858427

(50). Hetz C ; Bernasconi P ; Fisher J ; Lee AH ; Bassik MC ; Antonsson B ; Brandt GS ; Iwakoshi NN ; Schinzel A ; Glimcher LH ; Korsmeyer SJ Science 2006, 312, 572.16645094

(51). Urra H ; Hetz C Nat. Struct. Mol. Biol 2017, 24, 789;28981072Hetz C ; Papa FR Mol. Cell 2018, 69, 169.29107536

(52). Malhotra JD ; Miao H ; Zhang K ; Wolfson A ; Pennathur S ; Pipe SW ; Kaufman RJ Proc. Natl. Acad. Sci. U. S. A 2008, 105, 18525.19011102

(53). Sano R ; Reed JC Biochim. Biophys. Acta, Mol. Cell Res 2013, 1833, 3460.

(54). Lu M ; Lawrence DA ; Marsters S ; Acosta-Alvear D ; Kimmig P ; Mendez AS ; Paton AW ; Paton JC ; Walter P ; Ashkenazi A Science 2014, 345, 98.24994655

(55). Budihardjo I ; Oliver H ; Lutter M ; Luo X ; Wang XD Annu. Rev. Cell Dev. Biol 1999, 15, 269;10611963Li FZ ; Ambrosini G ; Chu EY ; Plescia J ; Tognin S ; Marchisio PC ; Altieri DC Nature 1998, 396, 580.9859993

(56). Fusco G ; Chen SW ; Williamson PTF ; Cascella R ; Perni M ; Jarvis JA ; Cecchi C ; Vendruscolo M ; Chiti F ; Cremades N ; Ying LM ; Dobson CM ; De Simone A Science 2017, 358, 1440;29242346Chiti F ; Dobson CM Annu. Rev. Biochem 2017, 86, 27.28498720

(57). Ogen-Shtern N ; Ben David T ; Lederkremer GZ Brain Res 2016, 1648, 658.27037184

(58). Teng P ; Niu Z ; She F ; Zhou M ; Sang P ; Gray GM ; Verma G ; Wojtas L ; van der Vaart A ; Ma S ; Cai J J. Am. Chem. Soc 2018, 140, 5661.29590526

(59). Vijayan D ; Young A ; Teng MWL ; Smyth MJ Nat. Rev. Cancer 2017, 17, 709.29059149

(60). Li S ; Mehta AK ; Sidorov AN ; Orlando TM ; Jiang Z ; Anthony NR ; Lynn DG J. Am. Chem. Soc 2016, 138, 3579;26942690Komaromy D ; Stuart MCA ; Santiago GM ; Tezcan M ; Krasnikov VV ; Otto S J. Am. Chem. Soc 2017, 139, 6234.28398730

(61). Wang H ; Luo Z ; Wang Y ; He T ; Yang C ; Ren C ; Ma L ; Gong C ; Li X ; Yang Z Adv. Funct. Mater 2016, 26, 1822;Zhan J ; Cai YB ; He SS ; Wang L ; Yang ZM Angew. Chem., Int. Ed 2018, 57, 1813;Lock LL ; Reyes CD ; Zhang P ; Cui H J. Am. Chem. Soc 2016, 138, 3533;26890853Zheng Z ; Chen P ; Xie M ; Wu C ; Luo Y ; Wang W ; Jiang J ; Liang G J. Am. Chem. Soc 2016, 138, 11128;27532322Yuan Y ; Wang F ; Tang W ; Ding Z ; Wang L ; Liang L ; Zheng Z ; Zhang H ; Liang G ACS Nano 2016, 10, 7147;27348334Yoshii T ; Mizusawa K ; Takaoka Y ; Hamachi I J. Am. Chem. Soc 2014, 136, 16635.25361466

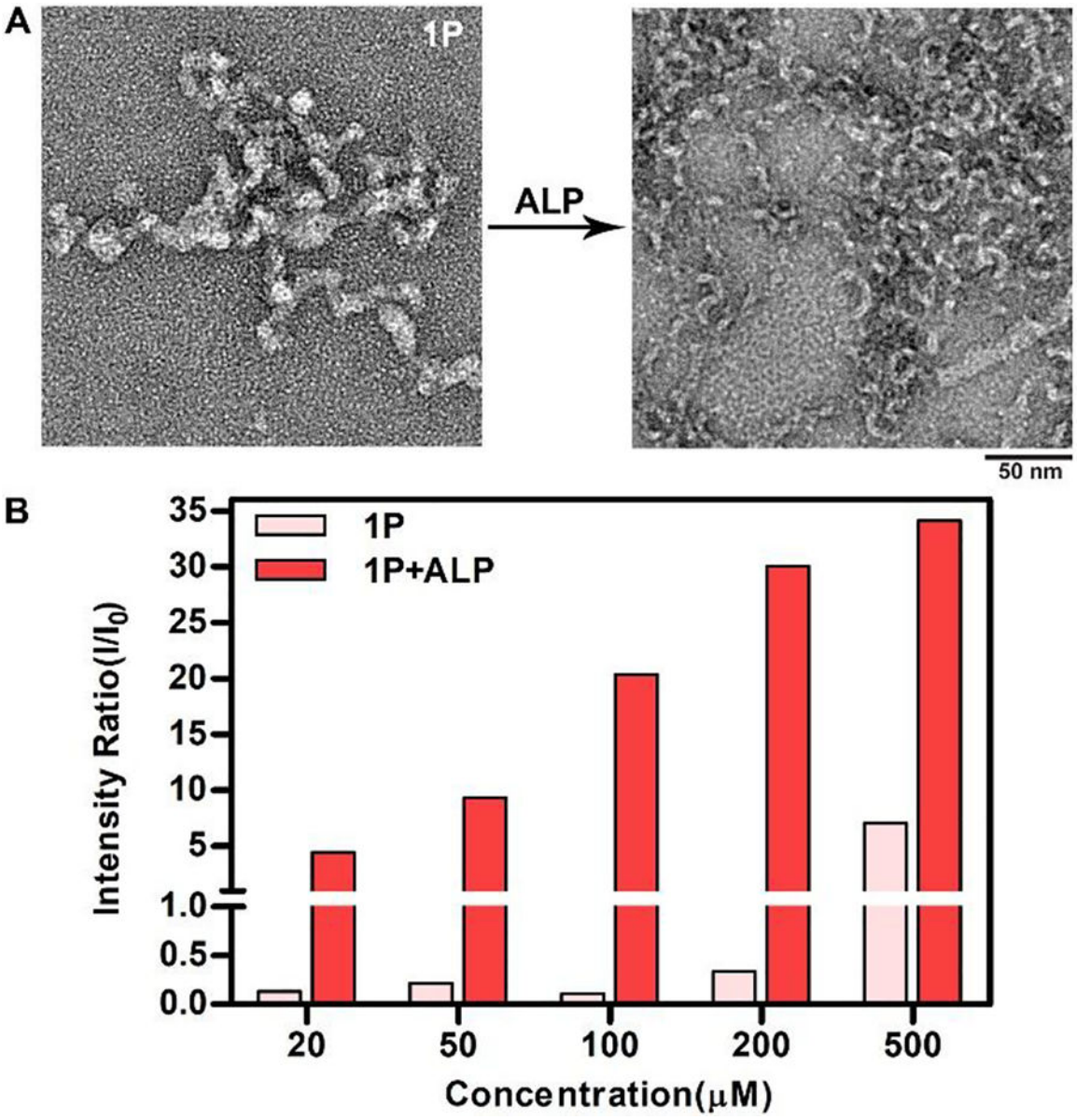


**Figure 1.**

(A) HRTEM image of nanostructures formed before and after adding ALP (1 U/mL) to the solution of **1P** (0.5 wt%, scale bar = 50 nm). (B) Intensity of static light scattering (SLS) of the solutions of **1P** (20–500 μM) before and after adding ALP (1 U/mL) for 12 h in pH 7.4 PBS buffer (light scattering angle = 30 degrees).

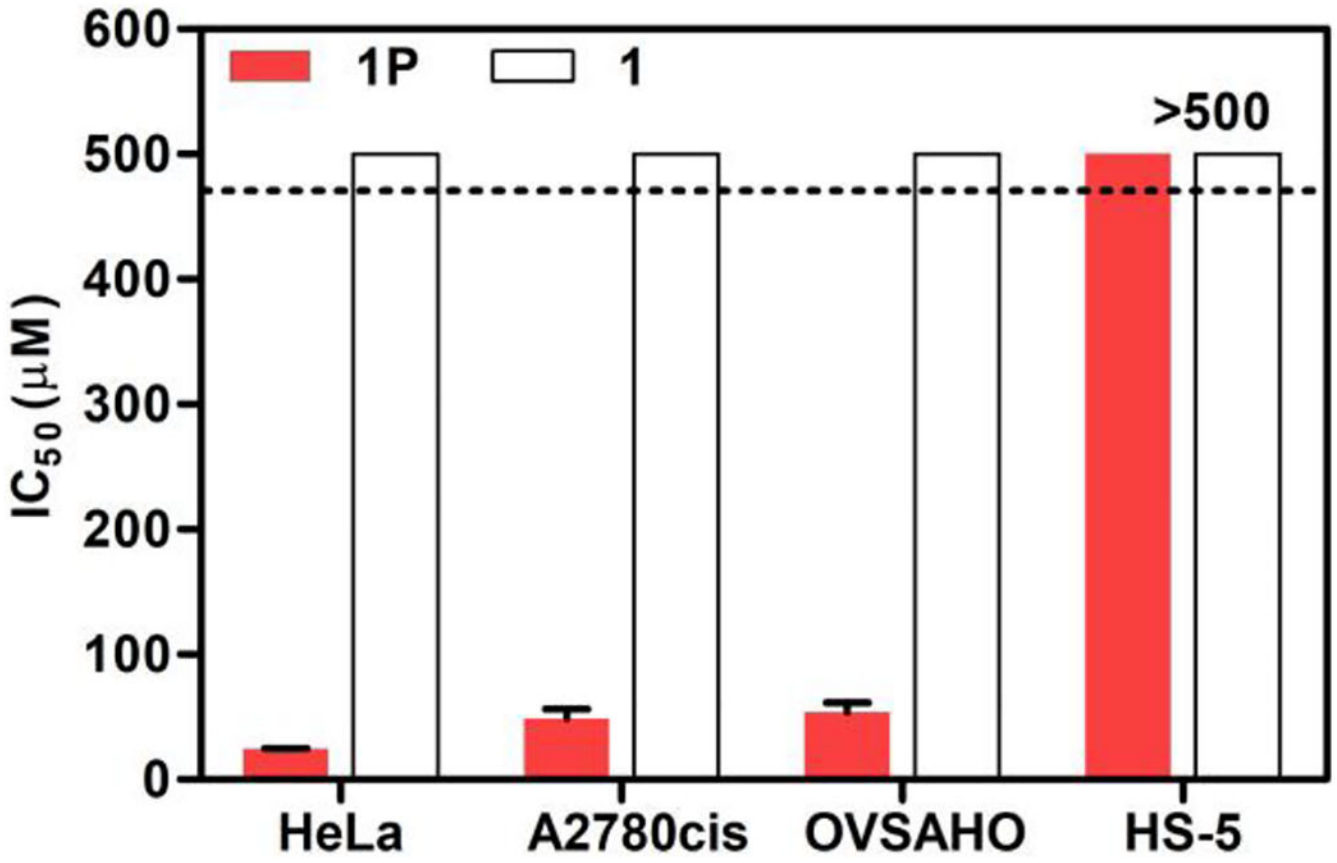


**Figure 2.**
The $IC_{50}$ (24 h) of **1P** or **1** against HeLa cells, A2780cis cells, OVSAHO cells, and HS-5 cells.

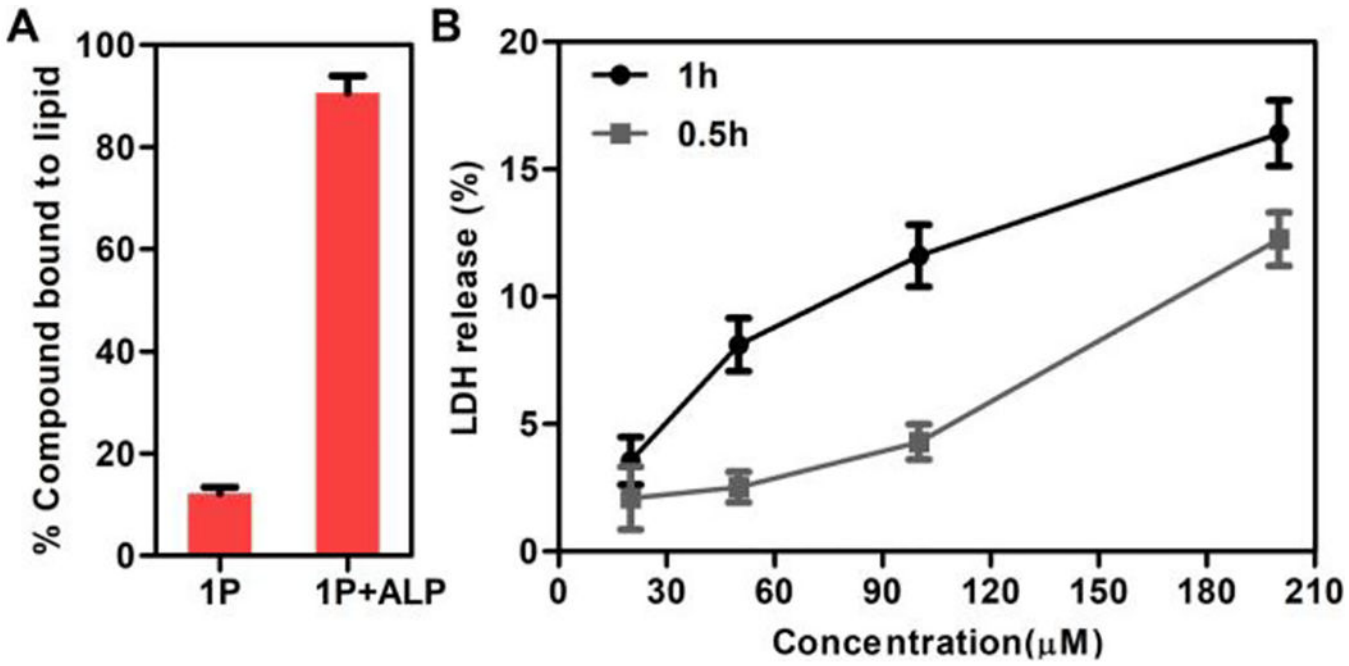


**Figure 3.**

(A) The liposome binding capability of **1P** (20 μM**)**, with or without the treatment of ALP. (B) Time dependent LDH release from the HeLa cells treated with **1P** at different concentrations. Data in both (A) and (B) obtained by triplicate measurements (n = 3) and presented as mean ± SEM.

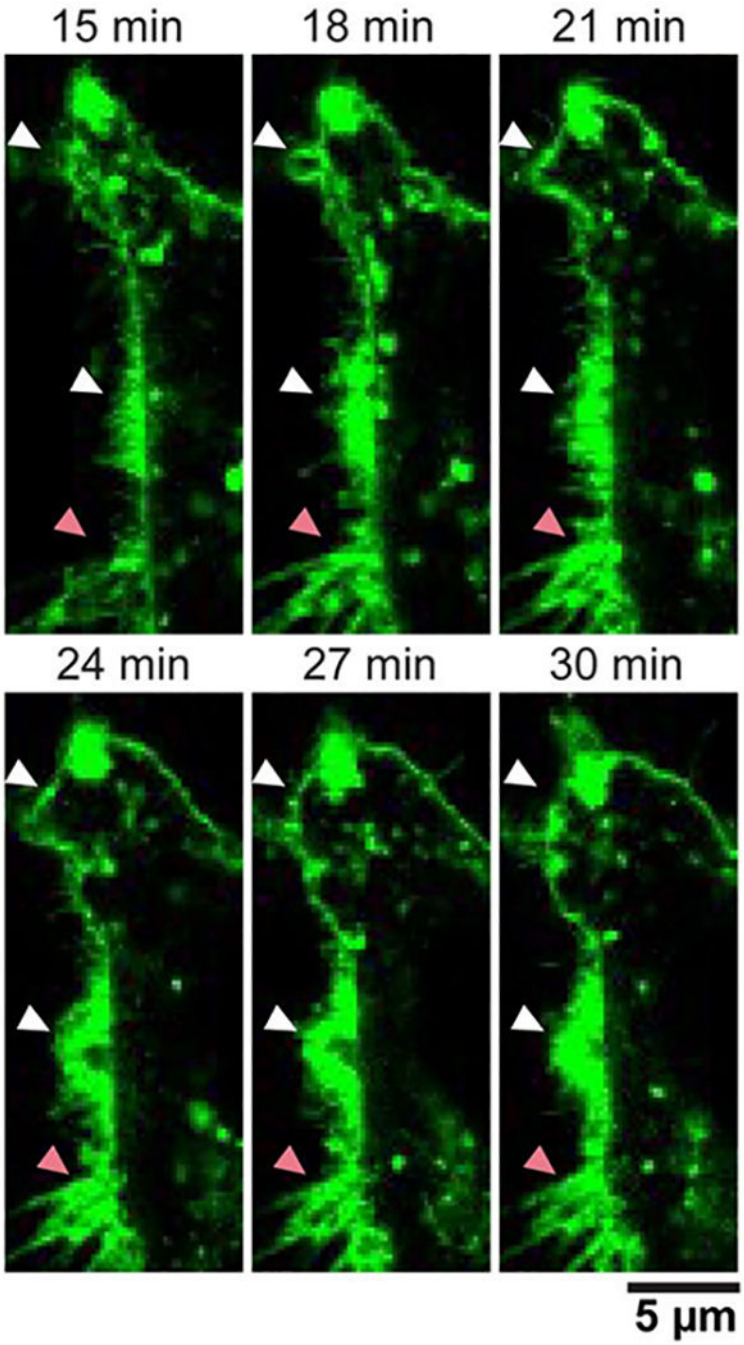


**Figure 4.**

Time-lapse microscopy images of live HeLa cells after incubation with **1P** (200 μM) for 15 to 30 minutes, showing the dynamic disruption of cell membrane (arrows). Before incubating with **1P**, the membranes of HeLa cells were stained with an active membrane probe[39] (10 μM) for 1 h.

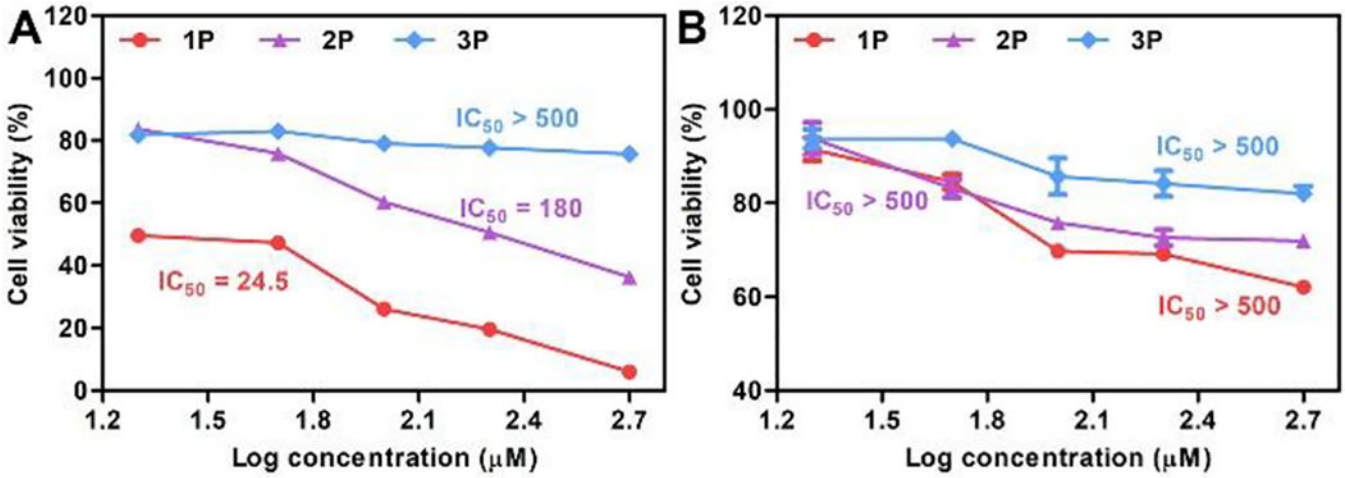


**Figure 5.**
Cell viability of (A) HeLa and (B) HS-5 cells treated with **1P**, **2P**, or **3P** for 24 h.

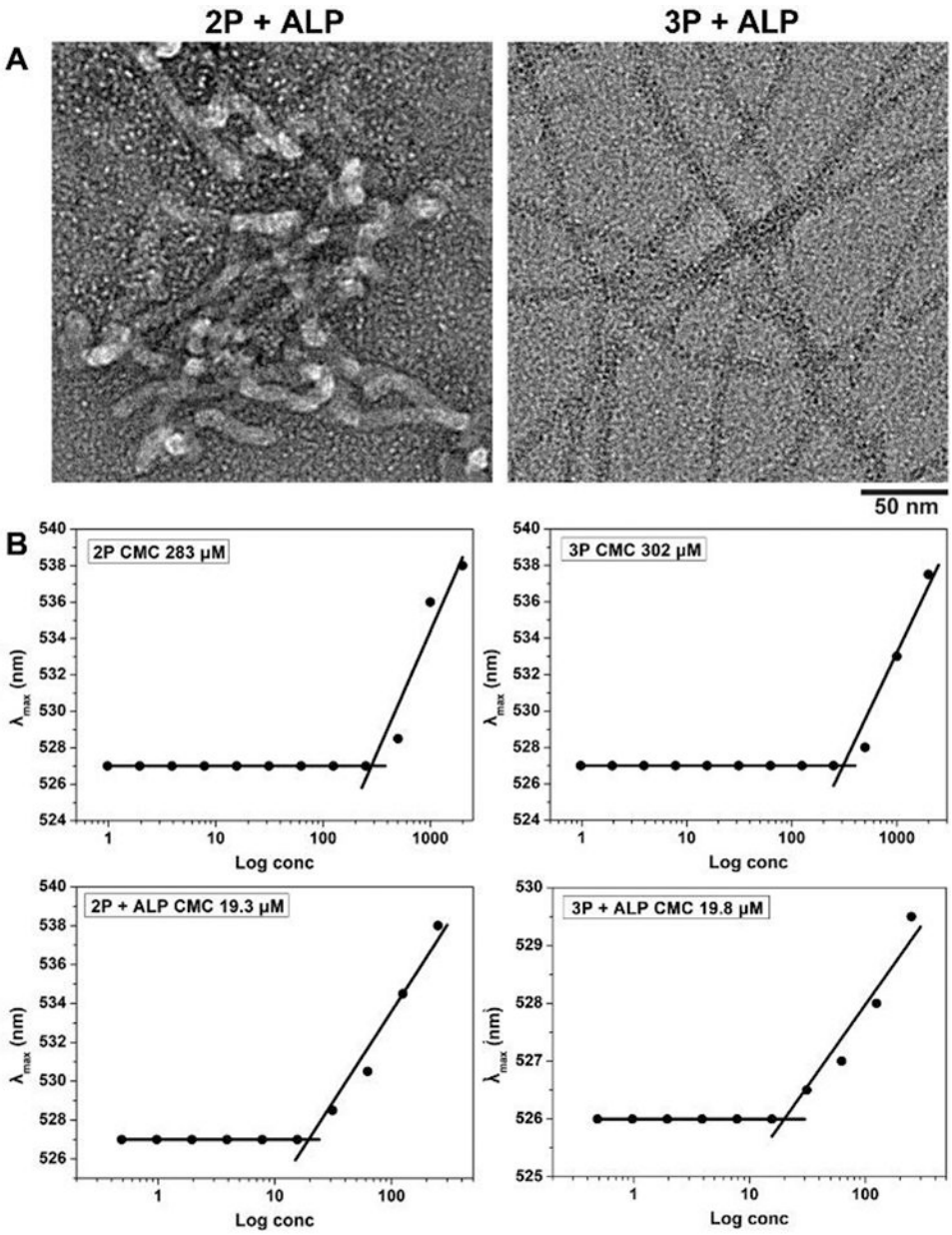


**Figure 6.**

(A) HRTEM images of the nanostructures formed by adding ALP to the solutions of **2P** (left) and **3P** (right) (0.5 wt%, scale bar = 50 nm); (B) CMCs for **2P** and **3P**, without or with the treatment of ALP.

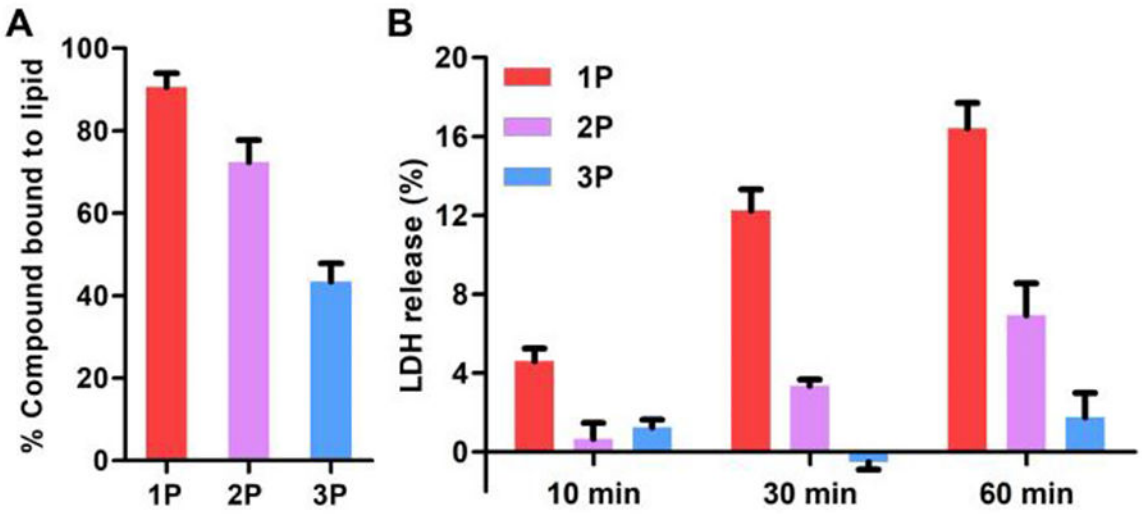


**Figure 7.**

(A) The liposome binding capability of **1P**, **2P** or **3P** (20 μM) after the treatment of ALP; (B) Time dependent LDH release of HeLa cells after treated with **1P**, **2P** or **3P** at 200 μM. Data in both (A) and (B) obtained by triplicate measurements (n = 3) and presented as mean ± SEM.

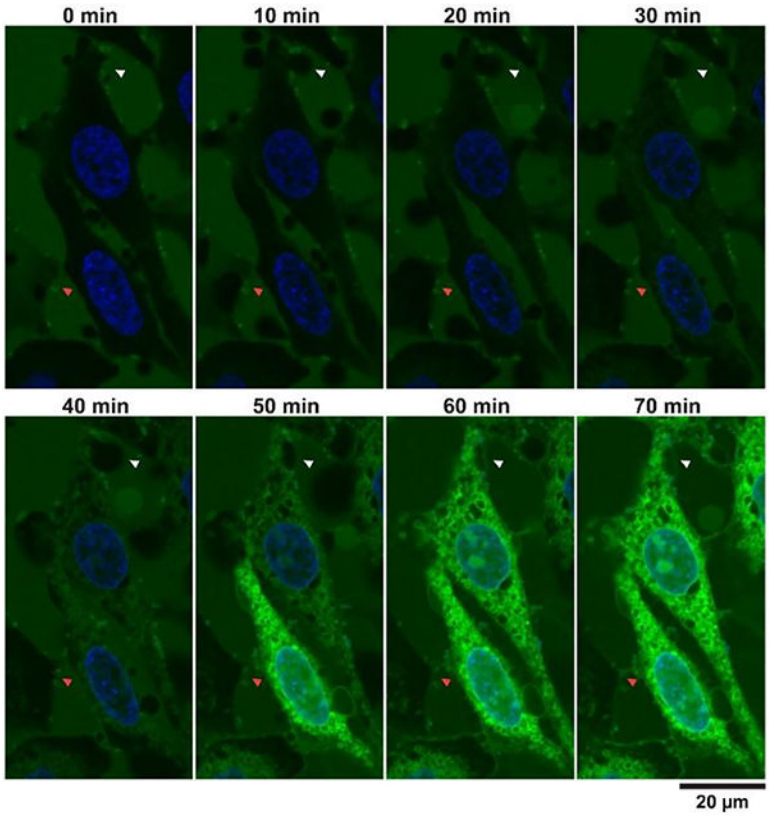


**Figure 8.**

Time-lapse microscopy images of live HeLa cells incubating with **F1P** (200 μM) for 0 to 70 minutes, showing the in-situ generation of assemblies of **F1P** on cell membrane (pink arrow), membrane disruption (white arrow), and real time distribution in the HeLa cells. Before incubating with **F1P**, the nuclei of HeLa cells were stained with Hoechst 33342.

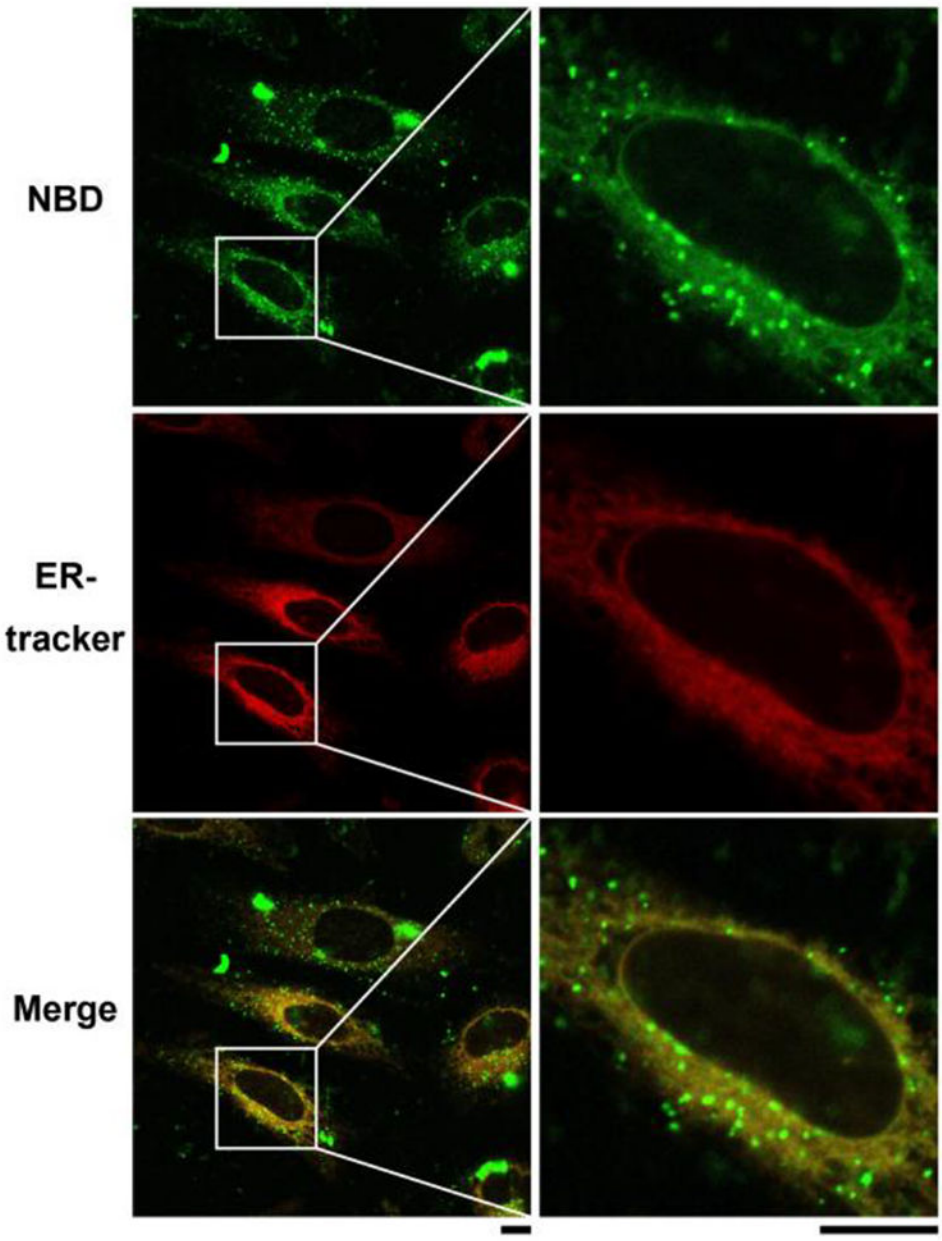


**Figure 9.**

Confocal laser scanning microscopy images of HeLa cells treated with **F1P** (200 μM) for 1 h, and then stained with ER-tracker. Scale bar is 10 μm.

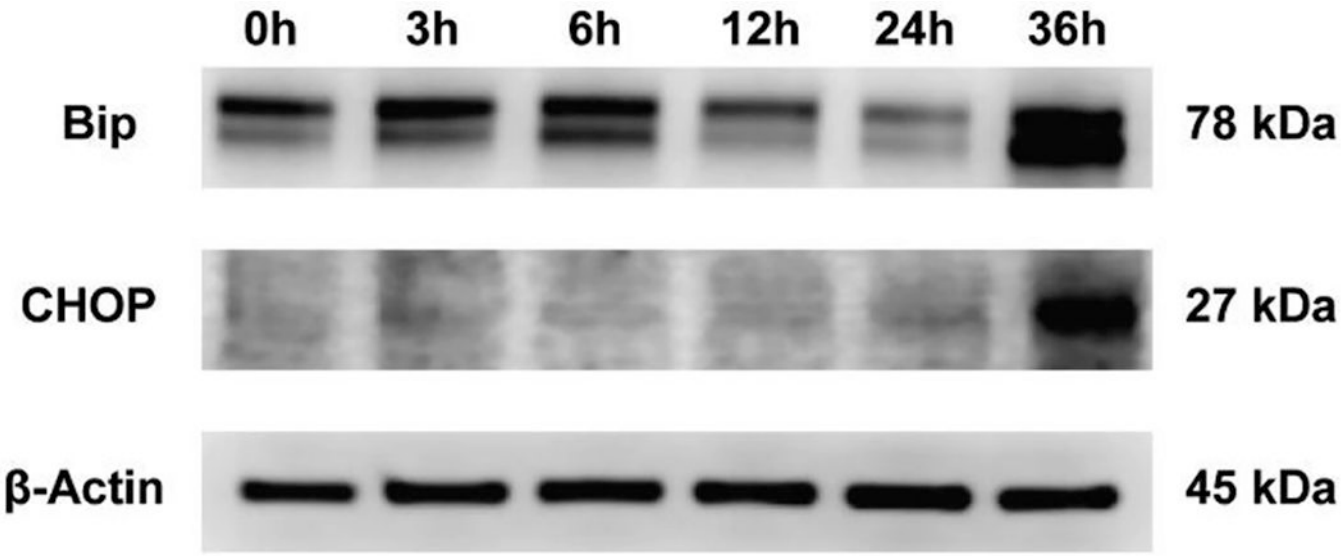


**Figure 10.**

Western blot analysis of ER-stress marker (Bip, CHOP) after treating HeLa cells with **1P** (50 μM) at different time (i.e., 0, 3, 6, 12, 24 or 36 h).

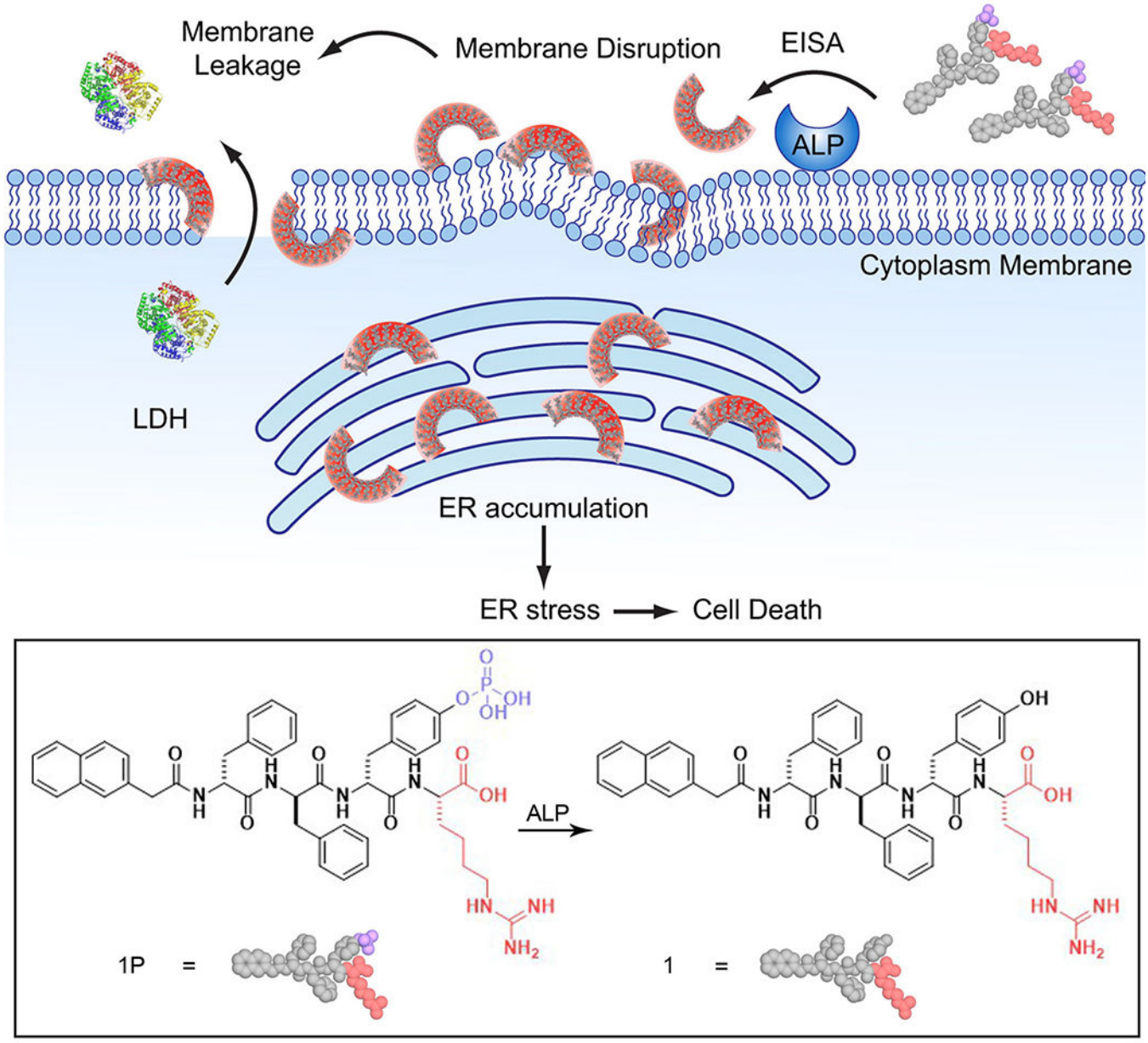


**Scheme 1.**

Illustration of EISA assemblies to disrupt cell membrane and to target ER and molecular structure of an EISA precursor.